1/f noise in solid-state nanopores is governed by access and surface regions

Fragasso, Alessio; Pud, Sergii; Dekker, Cees

DOI
10.1088/1361-6528/ab2d35

Publication date
2019

Document Version
Accepted author manuscript

Published in
Nanotechnology

1/f noise in solid-state nanopores is governed by access and surface regions

Alessio Fragasso, Sergii Pud, Cees Dekker

Department of Bionanoscience, Kavli Institute of Nanoscience, Delft University of Technology, Van der Maasweg 9, 2629 HZ Delft, The Netherlands.

Abstract

The performance of solid-state nanopores as promising biosensors is severely hampered by low-frequency 1/f noise in the through-pore ionic current recordings. Here, we develop a model for the 1/f noise in such nanopores, that, unlike previous reports, accounts for contributions from both the pore-cylinder, pore-surface, and access regions. To test our model, we present measurements of the open-pore current through solid-state nanopores of different diameters (1-50 nm). To describe the observed trends, it appears essential to include the access resistance in the modelling of the 1/f noise. We attribute a different Hooge constant for the charge carrier fluctuations occurring in the bulk electrolyte and at the pore surface. The model reported here can be used to accurately analyze different contributions to the nanopore low-frequency noise, rendering it a powerful tool for characterizing and comparing different membrane materials in terms of their 1/f-noise properties.

Solid-state nanopores are versatile single-molecule biosensors [1], [2], [3], [4] which hold great promise for bio-medical sensing [5]–[9] and sequencing [10]. The success of nanopores [11], [12], [13], [14] is due to their simplicity and elegant working principle, where upon passing the nanopore, single molecules induce the modulation of the through-pore ionic current, which can be detected by the electronics. Solid-state nanopores, i.e., small pores within a SiN membrane, can efficiently detect the analyte molecules [15], [16], read-out certain structural features of the detected molecules [8], [17], [18], and even discriminate short nucleotide sequences [19]. However, they still lack the precision of their biological counterparts, with which DNA sequencing has been achieved, either by direct reading of DNA bases [20],[21], or by sequencing-by-synthesis techniques [22]–[24]. This is due to the large translocation speeds [25], [26] and the sizeable ionic current noise [27]. Indeed, for many applications [25], [28], [29] the ionic current noise is a limiting factor.

The ionic current noise in solid-state nanopores originates from multiple sources, viz., the nanopore chip substrate, the membrane dielectric properties, the interface between the nanopore surface and the electrolyte solution, and the bulk of the electrolyte [30], [31]. An in-depth overview of noise spectroscopy and its application for nanopore sensors can be found in [32], [33]. Briefly, the high-frequency part of the ionic current noise arises from capacitance and dielectric loss of the chip [34] and thus can be engineered to lower values by chip design [34]–[36]. On the contrary, there is no established solution to dampen the low-frequency noise, which is mainly characterized by 1/f noise [31], the nature of which is poorly understood. Chen *et al.* [37] demonstrated that atomically thin films of aluminum oxide deposited onto the nanopore surface can suppress low-frequency noise in solid-state nanopores, but notably the initial noise that they had as a starting point in their experiments was extremely high as compared to the values commonly measured for bare silicon nitride [31], [35]. Smeets *et al.* [31] established that 1/f noise in nanopores obeys Hooge's empirical equation which relates the noise to the number of charge carriers in the pore volume. Wen *et al.* [38] further investigated the 1/f noise in solid-state nanopores, by analyzing pore-surface and pore-cylinder 1/f noise contributions as a function of pH and salt concentration. However, despite some success in describing the 1/f noise behaviour at different electrolyte conditions, none of these models so far has been able to quantitatively account for the 1/f noise for different nanopore geometries and membrane materials. This lack of a general theory to describe the noise hinders the analysis and search for low-noise nanopore materials and the development of methods for 1/f noise

suppression. Indeed, a comprehensive model capable of predicting 1/f noise behavior of solid-state nanopore sensors is very much welcome for further improvement of the sensor ionic-current measurement resolution.

Here, we present a general theoretical noise model for nanopores that, unlike previous reports, accounts for contributions from both the pore-cylinder, pore-surface, and access regions, as indicated in Figure 1A. Furthermore, we present experimentally measured values of the 1/f noise in SiN solid-state nanopores of different diameters (1-50 nm), and we find an excellent agreement between the model and the data. We show that the dependence of 1/f noise on geometrical parameters of the pores is governed by the distribution of the electric potential between the nanopore and the access region, which has been previously defined [39] and measured for different nanopore systems [40], [41]. Fitting the model to our experimental data, we deduce that the 1/f noise generated by the bulk (access and pore-cylinder) and surface regions stem from different noise mechanisms and should be described by distinct Hooge constants that differ by more than 3 orders of magnitude. We find that the surface noise dominates the nanopore noise for small pores up to 20 nm in diameter, which emphasizes the importance of surface properties for the nanopore performance. For larger pores, the access resistance dominates the noise properties. Our findings provide a framework for a fair comparison of the low-frequency properties of different membrane materials for nanopore experiments and thus may be of use in the search for new approaches to minimize 1/f noise in solid-state nanopores.

We develop our model for the low-frequency ionic current noise of the nanopore system based on the equivalent electric circuit of the nanopore, see Fig. 1B. The access region is modelled as a resistor (R_{acc}) that is connected in series to the resistances of the pore-cylinder (R_{cyl}) and pore surface (R_{surf}) that are connected in parallel. R_{cyl} accounts for the dissipative transport of ions in the cylindrical volume of the nanopore, whereas R_{surf} accounts for the contribution of the counterions that are shielding the nanopore surface charge [42].

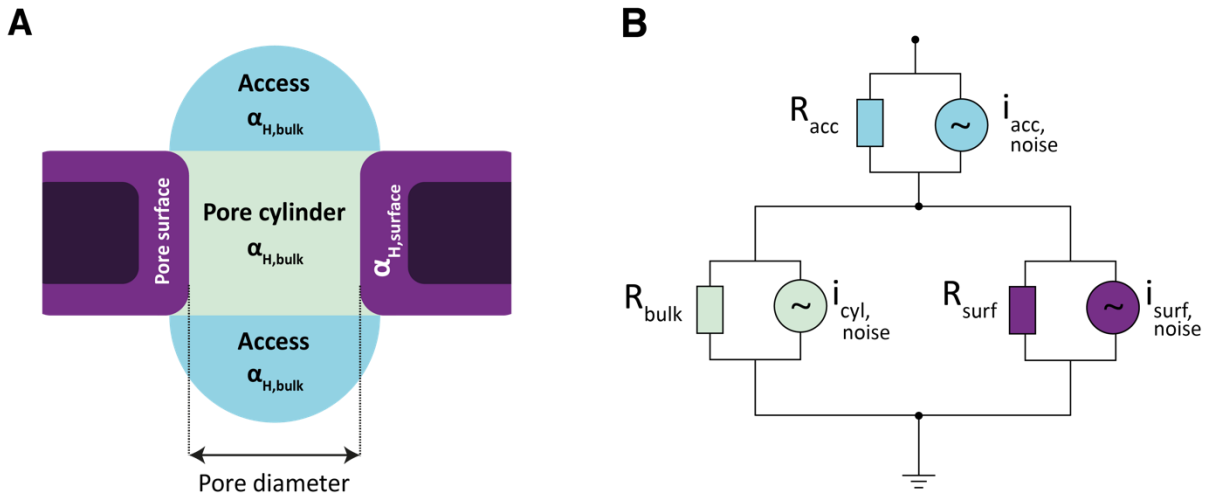

Figure 1. (A) Schematic representation of the relevant nanopore regions: access region (blue), pore-cylinder region (green), pore-surface (purple). (B) Equivalent circuit of the nanopore sensor. Nanopore regions are modelled as resistive elements connected in parallel to noise current generators.

We thus define

$$R_{pore} = R_{surf} || R_{cyl} \,, \tag{1}$$

$$R_{tot} = R_{pore} + R_{acc} \,. \tag{2}$$

From basic considerations of ion mobilities and geometry [41], [42], these resistances can be expressed as

$$R_{acc} = \frac{1}{ecN_A(\mu_{Cl^-}+\mu_{K^+})d} \,, \tag{3}$$

$$R_{cyl} = \frac{4L}{\pi ecN_A(\mu_{Cl^-}+\mu_{K^+})d^2} \,, \tag{4}$$

$$R_{surf} = \frac{L}{\pi\sigma_{surf}\mu_{K^+}d} \,, \tag{5}$$

where L is the membrane thickness (approximated as L = 8.6 nm due to the hourglass shape of the nanopore [43]), d is the diameter, e is the electron charge, c is the molar concentration of

the electrolyte, N_A is the Avogadro's number, μ_{Cl^-} and μ_{K^+} are the carrier mobilities, and σ_{surf} is the surface charge density.

Noise sources are modelled as noise-current generators that are connected in parallel to the noiseless resistors. The total current noise power spectral density $S_{I,tot}$ can now be expressed as

$$S_{I,tot} = S_{I,acc}\left(\frac{R_{acc}}{\mathrm{R}_{tot}}\right)^2 + (S_{I,cyl} + S_{I,surf})\left(\frac{R_{pore}}{\mathrm{R}_{tot}}\right)^2 \quad . \tag{6}$$

Derivation of Eq.6 is a result of application of Kirchoff's law for the circuit in Fig.1. In our model for the low-frequency noise, we consider only the 1/f noise for each of the nanopore regions (nanopore cylinder, nanopore surface, access region), which in each case is given by Hooge's model [44],

$$S_I = \frac{\alpha_H I^2}{N_c f} \quad , \tag{7}$$

where α_H is the Hooge parameter which is an empirical constant that indicates the strength of the 1/f noise, I is the dc current, N_c is the number of charge carriers participating in generating the ionic current, and f is the frequency. By measuring current fluctuations in bulk samples of different metals and semiconductors [44], Hooge found that low-frequency noise stems from fluctuations of sample conductance, which is inversely proportional to the amount of charge carriers. Importantly, this relation was found to suitably describe 1/f noise of the ionic current in solid-state nanopores [31], [38]. To account for the different contributions to the 1/f noise, the ionic currents and number of charge carriers need to be expressed separately for the three regions. We define the number of charge carriers present in the access region, $N_{c,acc}$, pore-cylinder region, $N_{c,cyl}$, and pore-surface region, $N_{c,surf}$, as

$$N_{c,acc} = \pi c N_A \frac{\mathrm{d}^3}{6} \quad , \tag{8}$$

$$N_{c,cyl} = \pi c N_A L \frac{d^2}{4} \quad , \tag{9}$$

$$N_{c,surf} = \pi \sigma_{surf} L \frac{d}{e} \quad , \tag{10}$$

where $N_{c,acc}$ is defined as the number of carriers in both hemispherical access regions (as shown in Figure 1A), which account for most of (~95%) the total 1/f noise occurring in the access regions (details in section SI6 of SI). Referring to the equivalent circuit model of Figure 1B, we can express the currents for the access I_{acc}, pore-cylinder I_{cyl}, and pore-surface I_{surf}, simply using Ohm's law and the voltage divider rule,

$$I_{acc} = \frac{V}{R_{tot}} \quad , \tag{11}$$

$$I_{cyl} = \frac{V_{cyl}}{R_{cyl}} = \frac{V}{R_{bulk}} \frac{R_{pore}}{R_{tot}} \quad , \tag{12}$$

$$I_{surf} = \frac{V_{surf}}{R_{surf}} = \frac{V}{R_{surf}} \frac{R_{pore}}{R_{tot}} \quad , \tag{13}$$

where V is the applied bias across the entire circuit. I_{surf} represents the current generated by the counterions adjacent to the pore walls. Since the conductance through such layer is different from the pore-cylinder it needs to be accounted as a separate term. To express the total 1/f current noise of the nanopore system, we substitute Equations (11-13) into Equation (7) to obtain

$$S_{I,acc} = \frac{\alpha_H {I_{acc}}^2}{N_{c,acc} f} = \frac{\alpha_{H,b}}{N_{c,acc} f} \frac{V^2}{R_{tot}^2} \quad , \tag{14}$$

$$S_{I,cyl} = \frac{\alpha_H {I_{cyl}}^2}{N_{c,cyl} f} = \frac{\alpha_{H,b}}{N_{c,cyl} f} \frac{V^2}{{R_{cyl}}^2} \frac{{R_{pore}}^2}{{R_{tot}}^2} \quad , \tag{15}$$

$$S_{I,surf} = \frac{\alpha_H {I_{surf}}^2}{N_{c,surf} f} = \frac{\alpha_{H,s}}{N_{c,surf} f} \frac{V^2}{{R_{surf}}^2} \frac{{R_{pore}}^2}{{R_{tot}}^2} \quad . \tag{16}$$

Finally, combining Equations (14-16) into (6), we can express the total 1/f noise $S_{I,tot}$ as

$$S_{I,tot} = \frac{V^2}{f {R_{tot}}^4} \frac{\alpha_{H,b} {R_{acc}}^2}{N_{c,acc}} + \frac{V^2}{f {R_{tot}}^4} \frac{\alpha_{H,b} {R_{pore}}^4}{{R_{cyl}}^2 N_{c,cyl}} + \frac{V^2}{f {R_{tot}}^4} \frac{\alpha_{H,s} {R_{pore}}^4}{{R_{surf}}^2 N_{c,surf}} \quad , \tag{17}$$

where $\alpha_{H,b}$ and $\alpha_{H,s}$ are the Hooge parameters for the bulk and surface 1/f noise. Note that this model has only two fit parameters $\alpha_{H,b}$ and $\alpha_{H,s}$ whereas all other quantities are given or can be calculated explicitly.

We experimentally tested this model by carefully examining the dependence of the 1/f noise on nanopore diameter, since the voltage drop over access and inner nanopore regions varies strongly with nanopore diameter (Eq.(3)-(5)). We thus prepared and studied a range of solid-state nanopores with sizes from 1.3 nm to 46 nm that were drilled within 20 nm-thick free-standing Si-supported membranes of silicon nitride using a transmission electron microscope (TEM). The details of the fabrication process and experimental setup are described elsewhere [45], [46]. Briefly, the membrane with a drilled nanopore was mounted into a microfluidic flow-cell, such that the nanopore was surrounded by two compartments filled with electrolyte solution. A buffer with 1 M KCl, 10 mM Tris-HCl, 1 mM EDTA, at pH 7 was used for measuring the ionic current through the nanopores. The ionic current through the nanopore was run using Ag/AgCl electrodes connected to an amplifier (Axopatch 200B, Axon Instruments) operating in resistive feedback mode. Current signals were acquired at a bandwidth of 100 kHz and digitized at 250 kHz. All experiments were performed at the room temperature. To ensure consistency, all chips were fabricated from the same wafer and handled equally. Nanopore diameters were calculated from the measured resistance (using Eq.S3), and generally found to be close (within 5-10%) to the values measured by TEM imaging (Figure 2A). Nanopores, which were hard to wet or that demonstrated an excessively noisy ionic current baseline (several orders of magnitude larger than across the whole set of nanopores) were excluded from the study. Ionic currents were recorded under a constant 100 mV applied bias. The power spectral density (PSD) of the ionic currents was computed over a time span of up to 60 seconds using a custom-written Matlab script. We fitted the spectra in the low-frequency range (<100 Hz) to extract the 1/f component. All fits were computed using the Matlab Curve Fitting Toolbox.

The acquired current power spectral density spectra are shown in Figure 2B. These are characteristic for nanopore noise behavior: at the low-frequency range, the 1/f noise dominates the PSD, then it transitions into a white noise region represented by shot and thermal noise, and subsequently into dielectric and capacitive noise for high-frequencies [47]. Notably, for pores larger than ~3 nm, the low-frequency noise decreases with increasing nanopore size. On the contrary, the white noise contribution, which we observe in the frequency range from 0.1-1 kHz, increases for larger pores. This is expected as the white noise, constituted by thermal and shot current noise scales linearly with the conductance G as

$$S_{I,white} = S_{I,thermal} + S_{I,shot} = G \cdot (4kT + 2Vq) \ , \tag{18}$$

where G is the total conductance, k is the Boltzmann constant, T is the absolute temperature in Kelvin (here 290 K), and q is the effective charge of the current carrying species. To extract the magnitude of 1/f noise from the PSD, we used a fitting function constituted by the sum of different low-frequency noise contributions, (Fig. 2C), namely

$$S_{I,tot}|_{f=1Hz} = S_{I,white} + \frac{A}{f} + \frac{B}{f^2} \ . \tag{19}$$

Here, the first term comprises the white noise contributions (i.e., both the thermal and shot noise), the second term represents the 1/f noise, and the third term accounts for a Lorentzian-shaped noise component, which is particularly pronounced in the smaller size nanopores. It can be attributed to fluctuations of the surface charge due to capture/release of ions from the electrolyte onto the nanopore surface [48]–[50]. This Lorentzian-shaped component is very slow (the characteristic crossover frequency is sub-1Hz) and unlike 1/f noise, is not inherent in all our nanopore data. It is not of major importance but is included in the fits to enable the most accurate determination of the 1/f noise level.

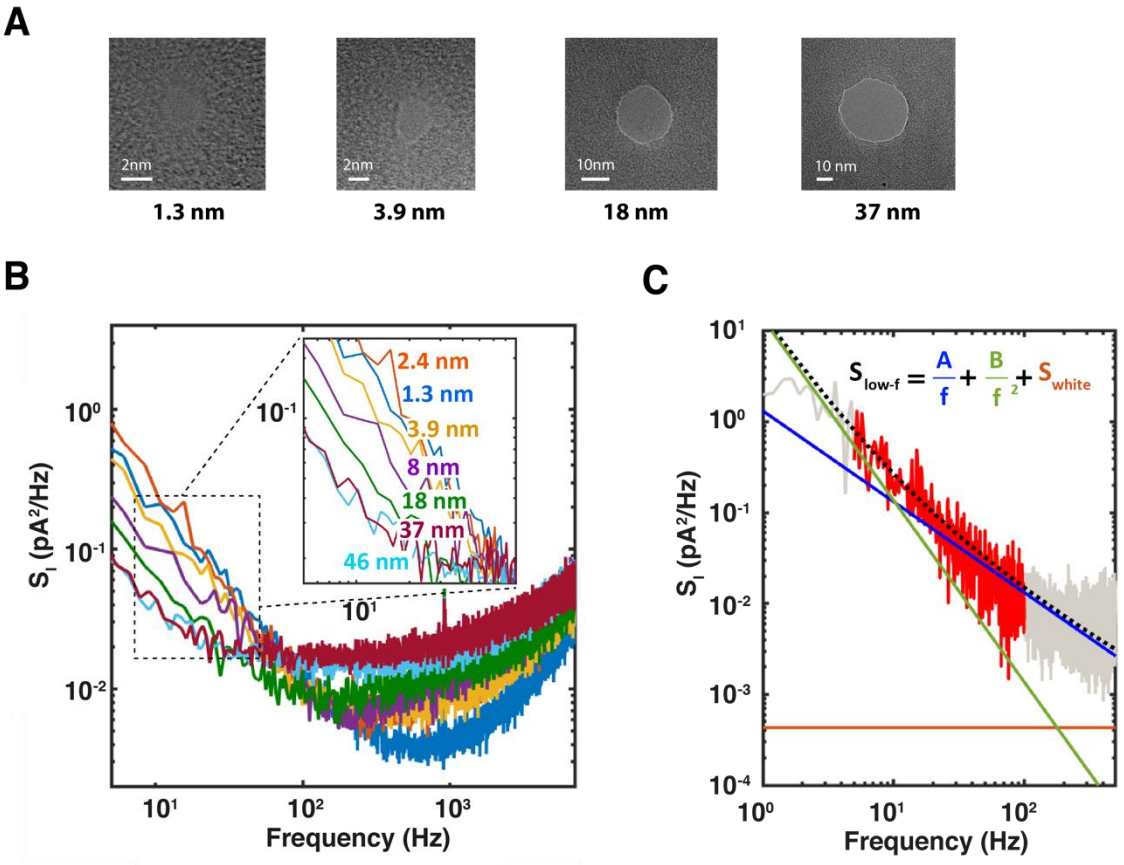

Figure 2. (A) TEM micrographs of the measured pores. Diameters were calculated from conductance measurements using Eq.S3. (B) Current power spectral density of nanopores with different diameters between 1.3 and 46 nm. The inset shows a zoom-in of the low frequency regions. (C) Example fit of the low-frequency ionic current power spectral density for a 2.4 nm pore. Dotted black line is the fit to the data (red) as reported by Equation (19), which comprises 1/f (blue), Lorentzian (green) and white noise (orange) contributions. The rest of the spectrum, out of the fitted region, is shown in light grey. Extracted values of A, B, and the calculated S_{white} are reported in Table (S1).

Note that the higher-frequency dielectric or capacitive noise contributions are not included into Equation (19) as their magnitude is negligible in the low-frequency range considered. By

contrast, the white noise needs to be taken into account, as it is not negligible for the large pores (>20 nm) in the 1-100 Hz range (Figure S2).

A major result of the current paper is presented in Fig. 3A which plots the extracted 1/f noise magnitudes versus nanopore size. We observe a decrease of 1/f noise of almost two orders of magnitude upon going from sub-5 nm pores to >40 nm diameter pores. Notably the variation in the 1/f noise is much weaker below a pore size of ~10 nm. To describe this behavior, we first consider previously developed models [27], [31], [38] that model the 1/f noise as coming only from the cylindrical nanopore, neglecting an access resistance contribution. Following this assumption, the total 1/f noise can be expressed [38] as

$$S_{I,pore} = \frac{\alpha_H {I_{surf}}^2}{N_{c,surf} f} + \frac{\alpha_H {I_{cyl}}^2}{N_{c,cyl} f} \quad , \tag{20}$$

where the first term describes the pore-surface 1/f noise, the second term describes the pore-cylinder 1/f noise, α_H is the (single) Hooge parameter, and I_{cyl}, $I_{surf,}$ $N_{c,cyl}$, and $N_{c,surf}$ are calculated explicitly using Equations (9-10) and (12-13). Equation (20) describes a monotonic increase of the magnitude of 1/f noise with pore size (for details, see SI), as illustrated by the green dashed line (Fig. 3A). Even qualitatively, this clearly contradicts our experimental observations and shows that it is crucial to take the access region into account to describe the size dependence of the 1/f noise. The pink line denotes such a model that accounts for the access resistance, where we have considered the simplest case of an equal Hooge parameter for the 1/f noise from the nanopore bulk and surface, i.e., we fitted Equation (17) to the data with $\alpha_{H,s} = \alpha_{H,b} = \alpha_H$ as the only fit parameter. This model qualitatively describes the trend of the data, but quantitatively clearly fails to fit well. However, by using two different Hooge constants for the 1/f noise at the surface of the nanopore and in the bulk of the electrolyte as fit parameters, an excellent fit to the experimental data can be obtained, as depicted by the purple line. This indicates that 1/f noise arising from the bulk and surface of the nanopore do differ substantially.

The decrease of the total 1/f noise for increasing pore diameter can be attributed to two underlying causes: (i) a voltage drop redistribution across access and pore region as determined by their resistances (Fig.1B), which strongly depend on the pore diameter (Eq.3-5): whereas the pore resistance dominates for smaller pore diameters, the access resistance dominates for

larger pores (Fig. S1); and (ii), the magnitude of 1/f fluctuations is much larger for the surface contribution than for the bulk noise. As a result of these two points, the surface 1/f noise dominates for small pores while the total 1/f noise decreases for larger pores where the weaker access noise dominates. From the fit, we find the surface and bulk Hooge parameters to be $\alpha_{H,s} = (2.1 \pm 0.2) \cdot 10^{-3}$ and $\alpha_{H,b} = (1.4 \pm 1.5) \cdot 10^{-6}$, respectively. Notably, the value we found for the surface noise coefficient is more than three orders of magnitude higher than the bulk value, showing that surface noise dominates. In passing we find it interesting to note that low-frequency noise studies in solid-state semiconductor devices also feature surface currents with a much higher Hooge parameter compared to the bulk ones [51] that arise from fluctuations of electrophoretic mobility of ions in the electrolyte [52]. Our value for $\alpha_{H,s}$ is also higher than the value of $\sim 1.1 \cdot 10^{-4}$ published previously for solid-state nanopores [31]. However, this value has been extracted using the `pore-only` model and represents a convolution between $\alpha_{H,s}$ and $\alpha_{H,b}$. If we calculate the α_H using a model as in [31] for a ~10 nm nanopore from our data set (similar size to the one used in [31]), then we find values that agree well with this reference.

A mechanism responsible for the high surface 1/f noise can possibly be charge carrier number fluctuations occurring at the pore-electrolyte interface due trapping at the surface. Whereas a single adsorption/dissociation process would lead to a Lorentzian noise spectrum, inhomogeneities at the pore surface will lead to a variety of trapping strengths which yields a 1/f spectrum [53], [48]. Such mechanism will strongly depend on the surface properties of the material (in this case SiN_x). 1/f noise measurements on solid-state nanopores fabricated from two different wafers (Fig. S3) yielded a factor 3 difference in $\alpha_{H,s}$, consistent with this notion. Obviously, our finding of the dominance of surface noise suggests strategies to lower the noise of nanopores, e.g. by surface engineering and choice of surface materials.

Figure 3B sketches the relative contributions of access, pore-cylinder, and pore-surface regions to the total 1/f noise $S_{I,tot}$. Using Eq. (6) and (14)-(17), the various colored lines plot the access $S_{I,acc} \left(\frac{R_{acc}}{\mathrm{R}_{tot}}\right)^2 / S_{I,tot}$ (blue), pore-cylinder $S_{I,cyl} \left(\frac{R_{pore}}{\mathrm{R}_{tot}}\right)^2 / S_{I,tot}$ (green), and pore-surface $S_{I,surf} \left(\frac{R_{pore}}{\mathrm{R}_{tot}}\right)^2 / S_{I,tot}$ (purple) contributions as a function of pore diameter. Clearly, the 1/f noise for small pores is dominated by surface noise, while for larger pores (> 20 nm) the noise mainly comes from the bulk noise associated with the nanopore access region. The latter may

appear remarkable given that its $\alpha_{H,b}$ is three orders of magnitude lower than $\alpha_{H,s}$, but is explained by the fact that the access resistance strongly dominates the pore resistance for pore diameters larger than 20 nm.

More generally, our model allows to quantify and predict 1/f noise behavior for nanopores of different geometries. It is clear that ultra-small pores (<5nm) are mainly showing surface 1/f noise and the large ones (>40 nm) mainly demonstrate the bulk noise of the access region. However, our model allows to quantify that the mid-range pores, which are most oftenly used for biosensing applications, still have a surprisingly strong contribution from the surface 1/f noise (Figure 3B). Therefore, the noise of these pores can be significantly improved by selection of the nanopore material or coating. Moreover, our model is also suitable for nanopores made in ultrathin membranes (e.g. 2D materials) and it predicts a lower 1/f current noise coming from the nanopore itself because of the major role of the access region even for the smaller nanopore diameters.

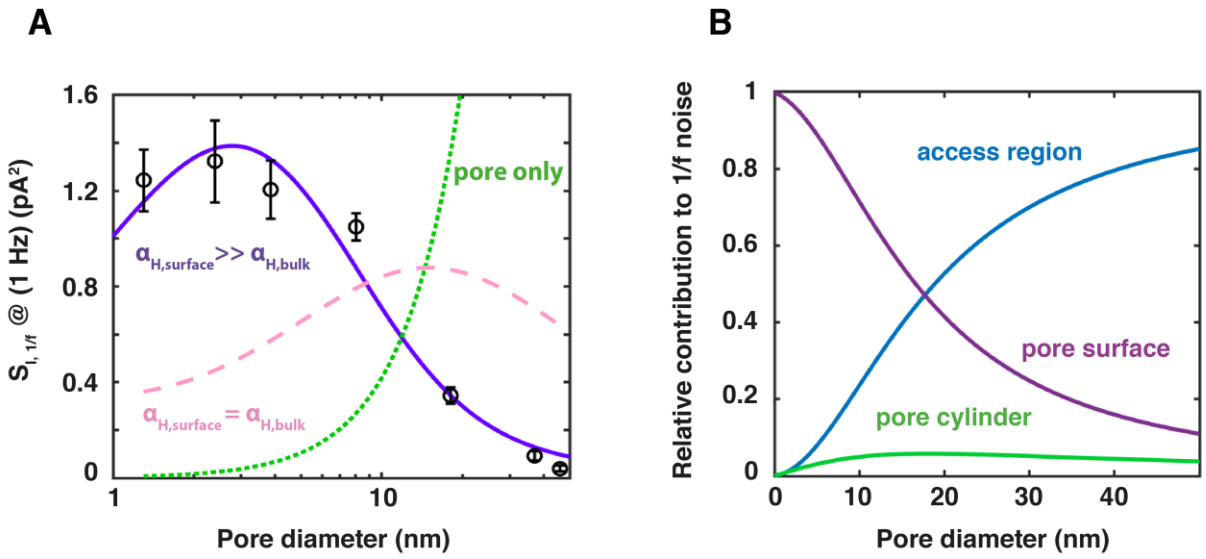

Figure 3. (A) Low-frequency 1/f noise plotted as a function of the pore diameter (black circles). We observe a decreasing trend of 1/f noise with increasing nanopore size, which spans more than one order of magnitude over the analyzed pore diameter range. Error bars represent standard deviations. The three lines represent model fits to the nanopore data: The green dotted line accounts for the model with no access resistance contribution; pink dashed line includes the access resistance, but treats 1/f noise as coming from one mechanism with a single Hooge parameter; and the purple curve shows the model comprising the access resistance and two independent Hooge parameters associated with bulk and surface noise. (B) Relative

contribution to the total 1/f noise originating from the three different nanopore regions: pore-surface (purple), pore-cylinder (green), and access region (blue), as a function of the nanopore diameter.

Summing up, we have developed a generalized predictive model for the 1/f noise in solid-state nanopores, which accounts for the dominant role of the access region of the nanopore sensor and for the different origins of 1/f noise in the solid-state nanopore. We find that 1/f noise of a solid-state nanopore derives from two sources, the nanopore surface and the bulk electrolyte, with Hooge parameters that differ by three orders of magnitude. Although the surface noise is more pronounced, the noise coming from the bulk electrolyte in the access region is the predominant source of noise for nanopore diameters larger than 20 nm. The developed model fits the experimental data remarkably well and can thus be used to compare 1/f noise performance of different nanopore materials. Importantly, it may be used to describe the 1/f noise for nanopores in very thin membranes, such as 2D-materials (graphene, boron nitride, molybdenum disulfide), where the access region is reported to dominate also for the smaller pore diameters.

Supplementary material

See supplementary material for the complete derivation of the models for the 1/f noise in nanopores, fitting to the current PSD, data extraction, other noise sources, and 1/f noise in the access region.

Acknowledgements

We would like to acknowledge Wayne Yang and Sonja Schmid for useful discussions, and Meng-Yue Wu for technical assistance on TEM. This work was supported by the National Human Genome Research Institute of the National Institute of Health under Award Number 1R01HG007406-01, by ERC Advanced grant SynDiv (no. 669598) and by the Netherlands Organisation for Scientific Research (NWO/OCW), as part of the NanoFront and BaSyC programs.

References

[1] C. Dekker, "Solid-state nanopores," *Nat. Nanotechnol.*, vol. 2, no. 4, pp. 209–216, 2007.

[2] Y. L. Ying, J. Zhang, R. Gao, and Y. T. Long, "Nanopore-based sequencing and detection of nucleic acids," *Angew. Chemie - Int. Ed.*, vol. 52, no. 50, pp. 13154–13161, 2013.

[3] X. Shi *et al.*, "Dynamics of a Molecular Plug Docked onto a Solid-State Nanopore," *J. Phys. Chem. Lett.*, vol. 9, no. 16, pp. 4686–4694, 2018.

[4] Y. Lin, Y. L. Ying, and Y. T. Long, "Nanopore confinement for electrochemical sensing at the single-molecule level," *Curr. Opin. Electrochem.*, vol. 7, pp. 172–178, 2018.

[5] E. Atas, A. Singer, and A. Meller, "DNA sequencing and bar-coding using solid-state nanopores," *Electrophoresis*, vol. 33, no. 23, pp. 3437–3447, 2012.

[6] A. H. Squires, J. S. Hersey, M. W. Grinstaff, and A. Meller, "A nanopore-nanofiber mesh biosensor to control DNA translocation," *J. Am. Chem. Soc.*, vol. 135, no. 44, pp. 16304–16307, 2013.

[7] B. N. Miles, A. P. Ivanov, K. a. Wilson, F. Doğan, D. Japrung, and J. B. Edel, "Single molecule sensing with solid-state nanopores: novel materials, methods, and applications," *Chem. Soc. Rev.*, vol. 42, no. 1, 2012.

[8] J. Y. Y. Sze, A. P. Ivanov, A. E. G. Cass, and J. B. Edel, "Single molecule multiplexed nanopore protein screening in human serum using aptamer modified DNA carriers," *Nat. Commun.*, vol. 8, no. 1, pp. 1–10, 2017.

[9] W. Yang *et al.*, "Detection of CRISPR-dCas9 on DNA with Solid-State Nanopores," *Nano Lett.*, vol. 18, no. 10, pp. 6469–6474, 2018.

[10] C. a. Merchant *et al.*, "DNA translocation through graphene nanopores," *Nano Lett.*, vol. 10, no. 8, pp. 2915–2921, 2010.

[11] S. Howorka and Z. Siwy, "Nanopore analytics: Sensing of single molecules," *Chem. Soc. Rev.*, vol. 38, no. 8, pp. 2360–2384, 2009.

[12] J. J. Kasianowicz, J. W. F. Robertson, E. R. Chan, J. E. Reiner, and V. M. Stanford, "Nanoscopic Porous Sensors," *Annu. Rev. Anal. Chem.*, vol. 1, no. 1, pp. 737–766, 2008.

[13] D. Deamer, M. Akeson, D. Branton, J. J. Kasianowicz, and S. M. Bezrukov, "Three decades of nanopore sequencing," *Nat. Biotechnol.*, vol. 34, no. 5, pp. 481–482, 2016.

[14] J. J. Kasianowicz and S. M. Bezrukov, "On 'three decades of nanopore sequencing,'"

Nat. Biotechnol., vol. 34, no. 5, pp. 481–482, 2016.

[15] R. Wei, V. Gatterdam, R. Wieneke, R. Tampé, and U. Rant, "Stochastic sensing of proteins with receptor-modified solid-state nanopores," *Nat. Nanotechnol.*, vol. 7, no. 4, pp. 257–263, 2012.

[16] L. Kapinos *et al.*, "Single-molecule transport across an individual biomimetic nuclear pore complex," *Nat. Nanotechnol.*, vol. 6, no. 7, pp. 433–438, 2011.

[17] N. A. W. Bell and U. F. Keyser, "Digitally encoded DNA nanostructures for multiplexed, single-molecule protein sensing with nanopores," *Nat. Nanotechnol.*, vol. 11, no. 7, pp. 645–651, 2016.

[18] C. Plesa *et al.*, "Direct observation of DNA knots using a solid-state nanopore," *Nat. Nanotechnol.*, no. August, pp. 1–6, 2016.

[19] K. Venta *et al.*, "Differentiation of short, single-stranded DNA homopolymers in solid-state nanopores," *ACS Nano*, vol. 7, no. 5, pp. 4629–4636, 2013.

[20] J. J. Kasianowicz, E. Brandin, D. Branton, and D. W. Deamer, "Characterization of individual polynucleotide molecules using a membrane channel," *Proc. Natl. Acad. Sci.*, vol. 93, no. 24, pp. 13770–13773, 2002.

[21] E. a Manrao *et al.*, "Reading DNA at single-nucleotide resolution with a mutant MspA nanopore and phi29 DNA polymerase," *Nat. Biotechnol.*, vol. 30, no. 4, pp. 349–353, 2012.

[22] S. Kumar *et al.*, "PEG-labeled nucleotides and nanopore detection for single molecule DNA sequencing by synthesis," *Sci. Rep.*, vol. 2, pp. 1–8, 2012.

[23] J. W. F. Robertson, C. G. Rodrigues, V. M. Stanford, K. A. Rubinson, O. V. Krasilnikov, and J. J. Kasianowicz, "Single-molecule mass spectrometry in solution using a solitary nanopore," *Proc. Natl. Acad. Sci.*, vol. 104, no. 20, pp. 8207–8211, 2007.

[24] C. W. Fuller *et al.*, "Real-time single-molecule electronic DNA sequencing by synthesis using polymer-tagged nucleotides on a nanopore array," *Proc. Natl. Acad. Sci.*, vol. 113, no. 19, pp. 5233–5238, 2016.

[25] C. Plesa, S. W. Kowalczyk, R. Zinsmeester, A. Y. Grosberg, Y. Rabin, and C. Dekker, "Fast translocation of proteins through solid-state nanopores," *Nano Lett.*, vol. 13, no. 2, pp. 658–663, 2013.

[26] A. J. Storm, C. Storm, J. Chen, H. Zandbergen, J. F. Joanny, and C. Dekker, "Fast DNA translocation through a solid-state nanopore," *Nano Lett.*, vol. 5, no. 7, pp. 1193–1197, 2005.

[27] R. M. M. Smeets, N. H. Dekker, and C. Dekker, “Low-frequency noise in solid-state nanopores,” *Nanotechnology*, vol. 20, no. 9, 2009.

[28] P. Ketterer *et al.*, “DNA origami scaffold for studying intrinsically disordered proteins of the nuclear pore complex,” *Nat. Commun.*, vol. 9, no. 1, pp. 1–8, 2018.

[29] S. J. Heerema, G. F. Schneider, M. Rozemuller, L. Vicarelli, H. W. Zandbergen, and C. Dekker, “1/F Noise in Graphene Nanopores,” *Nanotechnology*, vol. 26, no. 7, 2015.

[30] J. D. Uram, K. Ke, and M. L. Mayer, “Noise and bandwidth of current recordings from submicrometer pores and nanopores,” *ACS Nano*, vol. 2, no. 5, pp. 857–872, 2008.

[31] R. M. M. Smeets, U. F. Keyser, N. H. Dekker, and C. Dekker, “Noise in solid-state nanopores.,” *Proc. Natl. Acad. Sci. U. S. A.*, vol. 105, no. 2, pp. 417–21, 2008.

[32] Z. Roelen, J. A. Bustamante, A. Carlsen, A. Baker-Murray, and V. Tabard-Cossa, “Instrumentation for low noise nanopore-based ionic current recording under laser illumination,” *Rev. Sci. Instrum.*, vol. 89, no. 1, 2018.

[33] L. J. DeFelice, *Introduction to Membrane Noise*, 1st ed. Springer US, 1981.

[34] V. Tabard-Cossa, D. Trivedi, M. Wiggin, N. N. Jetha, and A. Marziali, “Noise analysis and reduction in solid-state nanopores,” *Nanotechnology*, vol. 18, no. 30, 2007.

[35] A. Balan, C. C. Chien, R. Engelke, and M. Drndic, “Suspended Solid-state Membranes on Glass Chips with Sub 1-pF Capacitance for Biomolecule Sensing Applications,” *Sci. Rep.*, vol. 5, no. September, pp. 1–8, 2015.

[36] K. B. Park *et al.*, “Noise and sensitivity characteristics of solid-state nanopores with a boron nitride 2-D membrane on a pyrex substrate,” *Nanoscale*, vol. 8, no. 10, pp. 5755–5763, 2016.

[37] P. Chen, T. Mitsui, D. B. Farmer, J. Golovchenko, R. G. Gordon, and D. Branton, “Atomic layer deposition to fine-tune the surface properties and diameters of fabricated nanopores,” *Nano Lett.*, vol. 4, no. 7, pp. 1333–1337, 2004.

[38] C. Wen *et al.*, “Generalized Noise Study of Solid-State Nanopores at Low Frequencies,” *ACS Sensors*, vol. 2, no. 2, pp. 300–307, 2017.

[39] J. E. Hall, “Access resistance of a small circular pore,” *J. Gen. Physiol.*, vol. 66, no. 4, pp. 531–532, 1975.

[40] S. M. Bezrukov, I. Vodyanoy, R. A. Brutyan, and J. J. Kasianowicz, “Dynamics and Free Energy of Polymers Partitioning into a Nanoscale Pore,” *Macromolecules*, vol. 29, pp. 8517–8522, 1996.

[41] S. W. Kowalczyk, A. Y. Grosberg, and Y. Rabin, “Modeling the conductance and DNA blockade of solid-state nanopores,” vol. 22, no. 315101, 2011.

[42] R. M. M. R. M. M. Smeets *et al.*, “Salt-dependence of ion transport and DNA translocation through solid-state nanopores,” *Nano Lett.*, vol. 6, no. 1, pp. 89–95, 2006.

[43] M. J. Kim, M. Wanunu, D. C. Bell, and A. Meller, “Rapid fabrication of uniformly sized nanopores and nanopore arrays for parallel DNA analysis,” *Adv. Mater.*, vol. 18, no. 23, pp. 3149–3153, 2006.

[44] F. N. Hooge, “1/F Noise,” *Phys. B+C*, vol. 83, no. 1, pp. 14–23, May 1976.

[45] X. J. a Janssen, M. P. Jonsson, C. Plesa, G. V Soni, C. Dekker, and N. H. Dekker, “Rapid manufacturing of low-noise membranes for nanopore sensors by trans-chip illumination lithography,” *Nanotechnology*, vol. 23, no. 47, p. 475302, 2012.

[46] M. van den Hout, A. R. Hall, M. Y. Wu, H. W. Zandbergen, C. Dekker, and N. H. Dekker, “Controlling nanopore size, shape and stability.,” *Nanotechnology*, vol. 21, no. 11, p. 115304, 2010.

[47] A. Balan *et al.*, “Improving signal-to-noise performance for DNA translocation in solid-state nanopores at MHz bandwidths,” *Nano Lett.*, vol. 14, no. 12, pp. 7215–7220, 2014.

[48] D. Zhang, P. Solomon, S. L. Zhang, and Z. Zhang, “An impedance model for the low-frequency noise originating from the dynamic hydrogen ion reactivity at the solid/liquid interface,” *Sensors Actuators, B Chem.*, vol. 254, pp. 363–369, 2018.

[49] S. Bezrukov and J. J. Kasianowicz, “Current Noise Reveals Protonation Kinetics and Number of Ionizable Sites in an Open Protein Ion Channel,” *Phys. Rev. Lett.*, vol. 70, no. 15, pp. 2352–2355, 1993.

[50] D. P. Hoogerheide, S. Garaj, and J. A. Golovchenko, “Probing surface charge fluctuations with solid-state nanopores,” *Phys. Rev. Lett.*, vol. 102, no. 25, pp. 5–8, 2009.

[51] L. K. J. Vandamme and D. Rigaud, “1/f noise in MOS devices, mobility or number fluctuations?,” *IEEE Trans. Electron Devices*, vol. 41, no. 11, pp. 1936–1945, 1994.

[52] R. P. Jindal and A. Van Der Ziel, “Model for mobility fluctuation 1/f noise,” *Appl. Phys. Lett.*, vol. 38, no. 4, pp. 290–291, 1981.

[53] P. Dutta and P. M. Horn, “Low-frequency fluctuations in solids: 1/f noise,” *Rev. Mod. Phys.*, vol. 53, no. 3, pp. 497–516, 1981.